

Protein Tertiary Structural Changes Visualized by Time-Resolved X-ray Solution Scattering

Sena Ahn, Kyung Hwan Kim, Youngmin Kim, Jeongho Kim, and Hyotcherl Ihee*

*Center for Time-Resolved Diffraction, Department of Chemistry, Graduate School of Nanoscience & Technology (WCU), KAIST, Daejeon 305-701, Korea**Received: July 23, 2009; Revised Manuscript Received: September 1, 2009*

We obtained a solution structural model of myoglobin (Mb) formed upon the CO photolysis of MbCO by analyzing time-resolved X-ray solution scattering data. An experiment-restrained rigid-body molecular dynamics simulation was used to find the best model whose theoretical difference scattering curve gives a satisfactory agreement with the experimental data at the time delay of 10 ns. The obtained solution model shows structural changes similar to crystallographic models for MbCO \rightarrow Mb but also displays a noticeable difference in that the N-terminus and F helix show larger structural changes.

Here, we report a transient solution structural model of myoglobin (Mb) formed 10 ns after the CO photolysis of MbCO. The model was obtained by analyzing experimental time-resolved X-ray solution scattering data with an experiment-restrained rigid-body molecular dynamics (MD) simulation. The root-mean-square deviation (rmsd) between Mb and MbCO is 0.2–0.3 Å,^{1,2} underscoring the high structural sensitivity of time-resolved X-ray solution scattering.

Knowledge of three-dimensional structures of proteins and their temporal progression is essential for understanding protein structure–function–dynamics relationships. Using short X-ray pulses from a synchrotron, a pump–probe time-resolved X-ray solution scattering technique was developed for tracking conformational changes of proteins in solution.^{3,4} The time resolution is in principle limited by the X-ray pulse width, which is currently 100 ps and will soon be improved to better than 0.1 ps upon the delivery of X-ray free electron lasers. Time-resolved X-ray solution scattering^{5–7} together with time-resolved X-ray crystallography⁸ can provide direct structural information, and thus complements time-resolved optical spectroscopy in the analysis of solution-phase reaction mechanisms. Moreover, time-resolved X-ray solution scattering complements time-resolved X-ray crystallography by probing the motions of proteins in their natural environment rather than in a single crystal.

Tertiary/quaternary structural transition in hemoglobin (Hb) was studied in depth with the time-resolved X-ray solution technique, and the kinetics and some preliminary structural analysis were given.³ It was also demonstrated that Mb shows a detectable difference scattering curve at the time delay of 10 ns upon the CO photolysis of carbonmonoxy Mb (MbCO), as shown in Figure 1A. This result for Mb is significant for the following reason. Hb consists of four subunits and thus large-amplitude quaternary (rearrangements of subunits) structural transitions as well as subtle tertiary (within a subunit) structural transitions are possible between liganded and unliganded states. In contrast, Mb is a single subunit and can accompany only subtle tertiary structural changes. For example, known crystal-

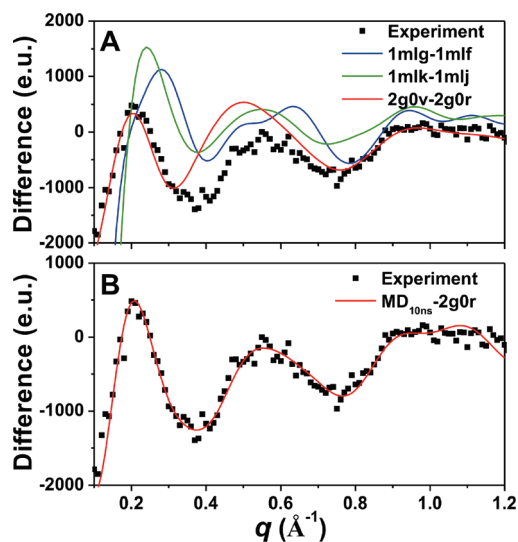


Figure 1. (A) Time-resolved X-ray solution scattering data at 10 ns for MbCO \rightarrow Mb in solution, and comparison with calculated difference curves (Mb – MbCO) where various known crystallographic models are used. (B) Experimental data and comparison with the difference scattering curve from a solution structural model for Mb (MD10ns) found from an experiment-restrained MD simulation and a reference crystallographic model for MbCO (2g0r).

lographic models of liganded and unliganded Hb show rmsd values ranging from 4 to 9 Å through the quaternary structural change,⁹ but the corresponding rmsd values between known crystallographic models of Mb and MbCO are less than 0.3 Å.^{1,2} The fact that the data for Mb shows clear oscillatory features (Figure 1A) supports the high structural sensitivity of time-resolved X-ray solution scattering, yet extracting structural information from the measured scattering data poses another challenge.

In Figure 1A, the experimental difference curve is compared with theoretical difference curves calculated by subtracting theoretical scattering curves for MbCO using X-ray crystallographic models from those for Mb using various known crystallographic models. Among numerous available crystal-

* To whom correspondence should be addressed. E-mail: hyotcherl.ihee@kaist.ac.kr.

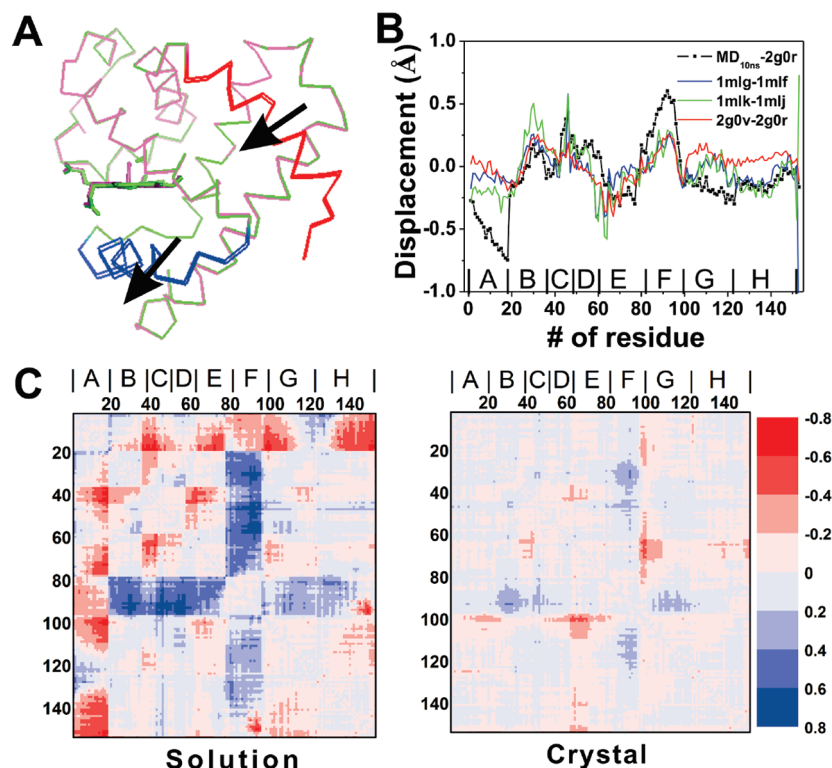


Figure 2. (A) Overlap of the obtained solution structure of Mb (green) and MbCO (magenta). The largest movements (indicated with arrows) are seen in the F helix (blue) and the A helix (red). (B) Displacement plot between the refined Mb structure (MD10ns) and MbCO (2g0r) as a function of amino acid sequence and comparison with those of crystal structures. Helices are labeled in the bottom. (C) Comparison of difference distance maps for solution and crystal: (left) a difference distance map between the refined solution Mb model obtained from experiment-restrained MD modeling and a reference crystallographic model for MbCO (2g0r); (right) that of crystal structures (2g0v–2g0r). Helices are labeled in the top.

lographic models, the three curves closest to the experimental curve are shown. Crystallographic models do not provide a satisfactory agreement with the experimental data, indicating that the solution structure deviates from them. In addition, crystallographic models also show some structural variations among themselves, as evidenced by the fact that different crystallographic models yield different scattering curves.

Normally, static X-ray scattering data is used for ab initio three-dimensional shape determination from the envelop model, bead model, and dummy-residue (DR) model.^{10–14} Recently, rigid-body modeling, where the tertiary structures are preserved, has been applied to construct multidomain proteins from solution scattering.¹⁵ This rigid-body modeling technique based on atomic structures uses known crystallographic models to calculate the scattering amplitude of the rigid-body that is determined by the atomic structures. In addition, Monte Carlo (MC) simulations using simulated annealing or restrained MD simulations are combined with modeling techniques to avoid being trapped in a local minimum in a refinement target function.^{10,16,17} These modeling methods provide a large convergence to find structures from the scattering data but require a priori assumptions, for example, known crystallographic models. In our structural modeling,⁴ we have used a similar experiment-restrained rigid-body MD approach that uses a priori knowledge based on the available crystallographic models. In our approach, the protein is divided^{15–19} into many (here we used eight) rigid bodies by grouping atoms belonging to one or two alpha helices into one rigid body. The heme is used as a separate rigid body. The difference between the calculated scattering curve and the experimental curve is used to calculate an MD force term in addition to the usual van der Waals force term. A time-resolved difference scattering curve rather than a static scattering curve

is used as the experimental curve. An MD simulation with simulated annealing runs until it reaches the best structure whose theoretical difference scattering curve gives satisfactory agreement with the experimental data. We fixed the MbCO structure at one of the crystallographic models for MbCO and refined the Mb structure by starting from one of the crystallographic models for Mb.

To check the validity of our rigid-body MD approach, we generated a mock difference curve by using two known structures for Mb and MbCO, also generated structural variants by modifying the original Mb structure, and used these modified structures as the starting structures. After rigid-body restrained MD simulations, the final structures converged to the correct structure with rmsd values less than 0.1 Å (Figure S1, Supporting Information),⁴ confirming that our procedure can find the global minimum faithfully.

After verifying that the restrained rigid-body MD simulation works for mock data, we applied it to the experimental data using various crystallographic models as starting structures (Figure S2, Supporting Information).⁴ The best agreement was obtained for the case where MbCO was fixed at 2g0r and Mb was fit starting from 2g0v: The result is shown in Figure 1B. The agreement is satisfactory up to 1 Å⁻¹. In Figure 2A, the obtained solution model of Mb and a crystallographic MbCO model are superimposed. The obtained solution structure provides us with the opportunity to compare it with the crystallographic model. Detailed structural features can be revealed with the aid of displacement plots (Figure 2B) and difference distance maps (Figure 2C). Displacement plots display the difference of distances between two structures as a function of the amino acid sequence and can reveal the subtle tertiary structural evolution of an Mb structure from a reference

MbCO structure. Here, the distance is from the center of the heme plane to the C α atom of each residue. Since the heme also moves a bit between MbCO and Mb, the absolute movement can be slightly biased in the displacement plot. The overall pattern of the solution model is similar to those of crystallographic models. The most well-known structural change for MbCO \rightarrow Mb is the clamshell movement where the E and F helices move downward relative to the position of the heme. The solution model also follows the same motion. However, there are also apparent differences in that the solution model shows a larger displacement in the A and F helices. This difference between the solution and crystallographic models is more vividly visualized in the difference distance map (Figure 2C) which plots the difference of the distance between any possible combinations of two C α atoms in the two different structures. It is evident that the solution model shows larger structural changes than the crystallographic model especially in the F helix in contact with the heme and at the A helix of the N-terminus. The N-terminus movement seems to be restricted in the crystal structure probably due to the crystal contact.

We also considered the effect of photoalignment induced by polarized excitation on the experimental data. The polarized laser light used in our measurement preferably dissociates the CO ligands of the hemes whose plane lies in the plane of the laser polarization. As a result, deoxy hemes and CO-bound hemes are transiently oriented in the polarization plane and perpendicular to the polarization plane, respectively. Then, this transiently oriented sample will undergo rotational diffusion, which, for Mb in solution, occurs on a similar time scale as the 10 ns time delay used in our measurement.²⁰ To account for this issue, we examined the photoalignment effect on the 1D X-ray scattering curve for a model system, namely, photodissociation of an iodine molecule. For this reaction, we simulated 2D scattering patterns by taking into account the fact that the probability of initial excitation is governed by the $\cos^2 \theta$ relationship (where θ stands for the angle of the laser polarization and the molecular dipole moment) (see Figure S3, Supporting Information). In other words, iodine molecules are anisotropically photoexcited. Clearly, due to the photoalignment effect, the 2D difference scattering image shows an anisotropic pattern and thus is different from that obtained with photoexcitation using unpolarized light (isotropic 2D pattern). However, if we convert these two different 2D images into 1D curves by integrating along the perimeter (as we did for our experimental scattering data), the anisotropic effect is completely wiped out and the resulting 1D curves are identical, as can be seen in Figure S3b (Supporting Information). This result clearly demonstrates that the photoalignment effect induced by polarized excitation is not reflected in the 1D curve and the reduction of a 2D image into a 1D curve simplifies the analysis of the measured kinetics. Thus, rotational diffusion of Mb molecules will not influence the structural dynamics retrieved from 1D curves, as in our work.

In summary, we obtained a solution structural model of Mb formed upon the CO photolysis of MbCO by analyzing time-resolved X-ray solution scattering data. Experiment-restrained rigid-body MD simulation was used to find the best model whose theoretical difference scattering curve gives satisfactory agreement with the experimental data at the time delay of 10 ns. The obtained solution model shows structural changes similar to crystallographic models but also displays a noticeable difference in that the N-terminus and F helix show larger structural changes.

Acknowledgment. This work was supported by the Creative Research Initiatives (Center for Time-Resolved Diffraction) of MEST/NRF.

Supporting Information Available: Detailed information on the X-ray scattering calculation and experiment-restrained rigid-body MD modeling. This material is available free of charge via the Internet at <http://pubs.acs.org>.

References and Notes

- (1) Quillin, M. L.; Li, T.; Olson, J. S.; Phillips, G. N., Jr.; Duo, Y.; Ikeda-Saito, M.; Regan, R.; Carlson, M.; Gibson, Q. H.; Li, H.; Elber, R. *J. Mol. Biol.* **1995**, *245*, 416.
- (2) Aranda, R.; Levin, E. J.; Schotte, F.; Anfinrud, P. A.; Phillips, G. N. *Acta Crystallogr., Sect. D* **2006**, *62*, 776.
- (3) Cammarata, M.; Levantino, M.; Schotte, F.; Anfinrud, P. A.; Ewald, F.; Choi, J.; Cupane, A.; Wulff, M.; Ihee, H. *Nat. Methods* **2008**, *5*, 881.
- (4) See the Supporting Information.
- (5) Haldrup, T.; Lemke, H. T.; Haldrup, K.; Nielsen, T. N.; Arms, D. A.; Walko, D. A.; Miceli, A.; Landahl, E. C.; Dufresne, E. M.; Nielsen, M. M. *J. Synchrotron Radiat.* **2009**, *16*, 387.
- (6) Ihee, H. *Acc. Chem. Res.* **2009**, *42*, 356.
- (7) Vincent, J.; Andersson, M.; Eklund, M.; Wohri, A. B.; Odellius, M.; Malmberg, E.; Kong, Q. Y.; Wulff, M.; Neutze, R.; Davidsson, J. *J. Chem. Phys.* **2009**, *130*, 154502.
- (8) Moffat, K. *Chem. Rev.* **2001**, *101*, 1569.
- (9) Silva, M. M.; Rogers, P. H.; Arnone, A. *J. Biol. Chem.* **1992**, *267*, 17248.
- (10) Svergun, D. I.; Petoukhov, V.; Koch, M. H. J. *Biophys. J.* **2001**, *80*, 2946.
- (11) Svergun, D. I.; Koch, M. H. J. *Curr. Opin. Struct. Biol.* **2002**, *12*, 654.
- (12) Chacon, P.; Moran, F.; Diaz, J. F.; Pantos, E.; Andreu, J. M. *Biophys. J.* **1998**, *74*, 2760.
- (13) Svergun, D. I. *Biophys. J.* **1999**, *76*, 2879.
- (14) Walther, D.; Cohen, F. E.; Doniach, S. *J. Appl. Crystallogr.* **2000**, *33*, 350.
- (15) Petoukhov, M. V.; Svergun, D. I. *Biophys. J.* **2005**, *89*, 1237.
- (16) Grishaev, A.; Wu, J.; Trewella, J.; Bax, A. *J. Am. Chem. Soc.* **2005**, *127*, 16621.
- (17) Kojima, M.; Timchenko, A. A.; Higo, J.; Ito, K.; Kihara, H.; Takahashi, K. *J. Appl. Crystallogr.* **2004**, *37*, 103.
- (18) Grossman, J. G.; Neu, M.; Pantos, E.; Schwab, F. J.; Evans, R. W.; Townes-Andrews, E.; Lindley, P. F.; Appel, H.; Thies, W.-G.; Hasnain, S. S. *J. Mol. Biol.* **1992**, *225*, 811.
- (19) Micetic, I.; Salvato, B. *Micron* **2004**, *35*, 17.
- (20) Wang, D.; Kreutzer, U.; Chung, Y.; Jue, T. *Biophys. J.* **1997**, *73*, 2764.

JP906983V